

Increasing force generation in electroadhesive devices through modelling of novel electrode geometries

BIGHARAZ, M. <<http://orcid.org/0000-0003-3285-3625>>, SCHENKEL, Torsten <<http://orcid.org/0000-0001-5560-1872>> and BINGHAM, Paul <<http://orcid.org/0000-0001-6017-0798>>

Available from Sheffield Hallam University Research Archive (SHURA) at:

<https://shura.shu.ac.uk/28446/>

This document is the Accepted Version [AM]

Citation:

BIGHARAZ, M., SCHENKEL, Torsten and BINGHAM, Paul (2020). Increasing force generation in electroadhesive devices through modelling of novel electrode geometries. *Journal of Electrostatics*, 109. [Article]

Copyright and re-use policy

See <http://shura.shu.ac.uk/information.html>

Increasing force generation in electroadhesive devices through modelling of novel electrode geometries

Masoud Bigharaz¹, Torsten Schenkel¹ and Paul A. Bingham¹

¹ Material and Engineering Research Institute, Sheffield Hallam University, City Campus, Howard Street, Sheffield S1 1WB, United Kingdom
E-mail: masoud.bigharaz@student.shu.ac.uk

Abstract

Two approaches were taken to increase the obtainable electroadhesive (EA) forces from EA electrode devices using finite element analysis (FEA): (i) optimising electrode widths and spacings using 2D parametric simulations; and (ii) optimising electrode geometries using 3D simulations. The Maxwell stress distributions generated by the simulated EA pads are reported; and illustrate how electrode geometries influence the EA forces generated. The FEA analyses were carried out using ANSYS MAXWELL with an automatic adaptive mesh refinement (AMR) technique which accelerates convergence and decreases the number of elements needed for study of mesh independency. The 2D parametric FEA shows optimum electrode widths of 2.6mm and optimum spacing between electrodes of 0.2mm for an effective surface of EA pads. 3D FEA shows that from the studied EA pads with a constant effective area, sine-wave shaped electrodes can generate substantially enhanced EA forces compared to other electrode geometries. This is attributed to maximising the electric field gradient and could benefit multiple applications. The simulation procedure is also validated by real-world problems.

Keywords: Electroadhesion, Finite element analysis, Maxwell stress tensor, Shape optimization, Mesh independency study

1. Introduction

Electroadhesion has received historical and recent attention due to its efficient performance in a variety of applications such as wall climbing robots [1, 2], and handling delicate materials [3-5]. It is also highly adaptable and capable of operating in many different environmental conditions, such as in space, air, and can generate attraction force on a wide range of materials including semiconductors and insulators [2]. Electrode adhesion is considered to be an ultra-low energy consumption technology, with power consumptions ranging from μW to mW [6, 7]. The components of an electroadhesion system are not complex (compared to some other adhesion mechanisms) and typically include a high voltage DC power supply; an EA pad; and a substrate (the material being adhered, such as a wall for wall climbing robots; or the object being picked up when EA pads are used as grippers). The structure of EA pads are very simple and usually consist of three layers: a backing material; electrodes; and a dielectric layer. Due to advances in electronic circuit fabrication processes, it is now possible to easily produce, even at lab-scale, rigid, semi-flexible, flexible and stretchable EA pads using cost-efficient methods [7-11].

Investigations have shown that the applied voltage, electrical properties and pattern/geometry of electrodes, electrical properties of the dielectric layer and substrate, as well as the thickness of the dielectric layer, are all important parameters affecting the obtainable EA force [12-14]. Investigations have therefore been carried out using different criteria to optimise EA pad performance: Guo *et al.* [9] have used total capacitance of system as a criterion to find optimised relationships between electrode width and spacing (width/space=1.8) to maximising normal force. Ruffatto *et al.* [12] used a gradient descent algorithm and the average electric field as a method of optimisation to maximise shear forces. In the present study, the effects of the variation of electrode geometry on Maxwell stress (EA force generated locally) were investigated with the aim of maximising the EA force, which builds upon and augments the above earlier work.

An EA force in a non-conductive material is produced through alignment of dipoles in the direction of an applied external electric field (polarisation) and is given by [15]:

$$\vec{P} = \epsilon_0 \chi_e \vec{E} \quad (1)$$

Where ϵ_0 is the permittivity of vacuum and equals to 8.85×10^{-12} F.m⁻¹; χ_e is polarizability of substance. In reality, χ_e is a tensor, but for simplification here it is considered as a scalar quantity; and E is the applied electric field in volts per meter (V/m).

Considering Z coordinate is perpendicular to the surface of an EA pad in the Cartesian system, the EA force is given by:

$$\vec{F}_z = \vec{P} \cdot \nabla \vec{E}_z \quad (2)$$

As in electrostatics an E-field is conservative Eq. (2) becomes:

$$\vec{F} = \nabla \left[\frac{1}{2} (\epsilon - \epsilon_0) \vec{E} \cdot \vec{E} \right] \quad (3)$$

By using the Divergence Theorem, the relationship between force and Maxwell stress tensor will be given by [16, 17]:

$$\iiint_V \vec{F} dV = \oint_S \vec{T} \cdot \vec{n} ds \quad (4)$$

where V is the volume of interest; T is the Maxwell stress tensor; and S is the boundary of the volume and n is a normal outward-facing vector.

The Maxwell stress tensor can be written as follows [18]:

$$T = \begin{bmatrix} \frac{\epsilon}{2} (E_x^2 - E_y^2 - E_z^2) & \epsilon E_x E_y E_z & \epsilon E_x E_y E_z \\ \epsilon E_x E_y E_z & \frac{\epsilon}{2} (E_y^2 - E_x^2 - E_z^2) & \epsilon E_x E_y E_z \\ \epsilon E_x E_y E_z & \epsilon E_x E_y E_z & \frac{\epsilon}{2} (E_z^2 - E_x^2 - E_y^2) \end{bmatrix} \quad (5)$$

The Maxwell stress generated on a substrate in the z -direction is shown in Figure 1; therefore the EA force is given by:

$$F_z = \oint_S \vec{T} \cdot \vec{n} ds = \iint_{A_z} T_{zz}^+ dA + \iint_{A_z} T_{zz}^- dA + \iint_{A_x} T_{xz}^{L1} dA - \iint_{A_x} T_{xz}^0 dA + \iint_{A_y} T_{yz}^{L2} dA - \iint_{A_y} T_{yz}^0 dA \quad (6)$$

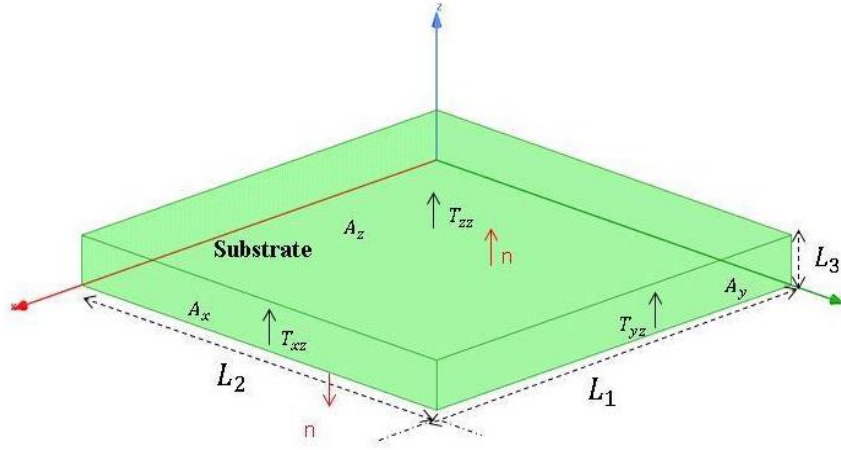


Figure 1. Maxwell stress on plans of a substrate in z direction

Where T_{zz}^+ is Maxwell stress in z-direction in the surface slightly above a substrate, T_{zz}^- is Maxwell stress in z-direction at the bottom surface of a substrate, T_{xz}^{L1} Maxwell stress in z direction at the front surface of a substrate, T_{xz}^0 Maxwell stress in z direction at the rear surface of a substrate, T_{yz}^{L2} Maxwell stress in z direction at the left surface of a substrate T_{yz}^0 Maxwell stress in z direction at the right surface of a substrate and because these surfaces are far away, the Maxwell stress can be neglected in all the surfaces (see figure(1)).

Therefore:

$$F_z = \iint_{A_z} T_{zz}^+ dA \quad (7)$$

According to the Eq. (2) the obtainable EA force can be increased by: (1) increasing intensity of the E-field which means increasing the applied DC voltage or by optimising the widths of electrodes and the spacing between adjacent electrodes; (2) maximising the gradient of the E-field by optimising the shape of the electrodes; and (3) improving electrical properties of the dielectric layer including increasing relative permittivity and dielectric strength.

2. Methodology

2.1. Finite element method

The finite element method (FEM) is a well-known numerical procedure to solve complicated partial differential equations (PDE) which cannot be solved using classical analytical methods due to the complexity of either PDE or geometry of interest. The FEM can be used to approximate the solutions to a wide variety of physical problems including solids, fluids, porous media or electromagnetic environments. Commercial and open-source software have now been developed that can simulate weakly- or strongly-coupled physical problems such as acoustic-structure interactions [19], fluid-structure interactions [20] and saturated porous media. The procedure for FEM analysis is to divide the geometry of interest into very small elements using different meshing techniques and to solve PDEs approximately within each element. Those PDEs that need to be solved in electrostatic field analysis are the Laplace and Poisson equations [21]. Researchers have shown that FEM is an effective method for electrostatic field analysis in two-dimensional (2D), axisymmetric and three-dimensional (3D) regions of interest with multiple dielectric media [14, 17 and 22].

In this study, numerical analyses were performed by considering the following assumptions:

- (1) Electrodes are perfect electrical conductors;

(2) Dielectric materials are linear, isotropic and homogenous (LIH). Linear dielectric materials are materials for which there is a linear relationship between their polarisation and the intensity of the electric field. Isotropic, in this context, means that their relative permittivities are not dependent upon direction:

$$\epsilon_x = \epsilon_y = \epsilon_z$$

(3) The power supply is a dual-polarity DC voltage;

(4) In 2D simulations, the electric field is constant in the y-direction, neglecting the marginal part of the EA pad (thus representing the central part of the electrode);

(5) Dielectrics do not have free charge density;

(6) EA pads are considered to be fully charged and the generated force is not time-dependent. We note that Bamber *et al.* [6] measured the electric potential distribution of an interdigitated EA pad with 230 mm x 190 mm effective area and their results showed that it took roughly 30 minutes for that pad to become fully charged.

(7) To simplify simulations and achieve mesh independent results, the effect of the backing plate is neglected and we assumed that electrodes are embedded exactly in the middle of a dielectric layer.

2.2. Simulation procedure in ANSYS Maxwell

ANSYS MAXWELL has been used to simulate electrostatic problems before [23, 24 and 25]. The simulation procedure includes three main steps: pre-processing, processing and post-processing. In the pre-processing step, first, the domain of interest is created including the electrode pattern, dielectric layer, air layer and substrate, and then the electrical properties of each material are added (electrodes are pure copper with perfect electrical conductivity, relative permittivity of dielectric, air and substrate) and finally, boundary conditions (B.C) are specified as follows:

(i) Potential difference for electrodes (Dirichlet boundary condition).

(ii) Interfacial boundary conditions between two layers with different relative permittivity (see Figure 2): electric potential and tangential orientation of the electric field is equal at the interface see Eq. (8, 9) and normal orientation of the electric field is varying according to Eq. (10).

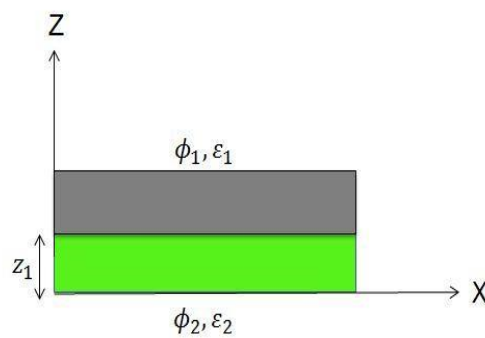


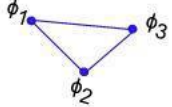
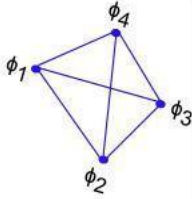
Figure 2. Definition of boundary conditions in Cartesian coordinates

Table 1. Types of B.C used for 2D and 3D simulation

2D B.C	3D B.C		
$\phi_1(x, z) = \phi_2(x, z)$	$\phi_1(x, y, z) = \phi_2(x, y, z)$	at $Z=z_1$	(8)
$\frac{\partial \phi_1(x, z)}{\partial x} = \frac{\partial \phi_2(x, z)}{\partial x}$	$\frac{\partial \phi_1(x, y, z)}{\partial x} = \frac{\partial \phi_2(x, y, z)}{\partial x}$ $\frac{\partial \phi_1(x, y, z)}{\partial y} = \frac{\partial \phi_2(x, y, z)}{\partial y}$	at $Z=z_1$	(9)
$\epsilon_1 \frac{\partial \phi_1(x, z)}{\partial z} = \epsilon_2 \frac{\partial \phi_2(x, z)}{\partial z}$	$\epsilon_1 \frac{\partial \phi_1(x, y, z)}{\partial z} = \epsilon_2 \frac{\partial \phi_2(x, y, z)}{\partial z}$	at $Z=z_1$	(10)

Where ϕ is electric potential and ϵ_1 and ϵ_2 are the relative permittivities of two different layers. In the processing step the region of interest is discretised to triangular elements for 2D simulations and tetrahedral elements for 3D simulations and it is assumed that electric potential is varying linearly within each element and also electric field in all directions are constant within each element (see Table 2).

Table 2. Types of elements available in ANSYS Maxwell, discretisation methods and calculation of potential energy

	Type of element	shape of element	Potential distribution at the corners of element	Electric field in element	Potential energy in element
2D	Triangular		$\phi_i = \alpha_1 + \alpha_2 x_i + \alpha_3 z_i$	$E_x = -\frac{\partial \phi}{\partial x} = -\alpha_2$ $E_z = -\frac{\partial \phi}{\partial z} = -\alpha_3$	$u_e = \frac{1}{2} \epsilon_0 \epsilon_r V (\alpha_2^2 + \alpha_3^2)$
3D	Tetrahedral		$\phi_i = \alpha_1 + \alpha_2 x_i + \alpha_3 y_i + \alpha_4 z_i$	$E_x = -\frac{\partial \phi}{\partial x} = -\alpha_2$ $E_y = -\frac{\partial \phi}{\partial y} = -\alpha_3$ $E_z = -\frac{\partial \phi}{\partial z} = -\alpha_4$	$u_e = \frac{1}{2} \epsilon_0 \epsilon_r V (\alpha_2^2 + \alpha_3^2 + \alpha_4^2)$

2.3. Hardware specifications for simulations

Electrode adhesion simulations using ANSYS MAXWELL are memory-bound which means the time needed to complete a simulation is mostly dependent upon the amount of memory required to hold data, so needs a “fat node” setup. Therefore, all simulations were performed on an 8-core Intel(r) Xeon(r) CPU E5-1620 v4 @ 3.50GHz workstation with 256 GB RAM. The simulation time for 2D parametric simulations with a particular electrode width and spacing was approximately 80 minutes and for a 3D simulation was approximately 50 hours.

2.4 Validation of the numerical method

In order to validate the numerical model and procedure, we compare our numerical model results with experimental data published by Dadkhah et al [8].

Dadkhah et al[8] Present electroadhesive pressures for uni-layer electrode systems using a variety of building materials including drywall, alder, poplar, adobe, painted aluminium and sandstone.

The numerical validation model consists of similar electrode patterns (0.4mm electrode width and 0.2mm electrodes spacing) as in the experimental setup (see figure5) with an effective area of 5.8 mm by 6.8 mm. Therefore the number of elements needed for mesh independency of the numerical results with thin layers of dielectric and a thin air gap between the EA pad and a substrate is achievable before meeting hardware limitations. The relative permittivity of the substrates was not given by Dadkhah et al., but typical values for similar materials range from 2 to 5.5 (Paper 2.3, Concrete 5.0, Wood, Dry 2-6 [26]).

The experimental results showed that the pressure generated by the uni-layer electrode varies between 0.2 and 1.2 kPa depending on the substrate. Figure 6 shows that the numerical model predicts electroadhesive pressures from 0.38 to 1.37 kPa matching the trend seen in the experimental results, while the numerical predictions are consistently slightly higher than the measured values. Considering the uncertainty in the published experimental data, in particular the lack of exact relative permittivity, the numerical model shows good agreement with the experimental results. The contour of Maxwell stress is presented in figure 7.

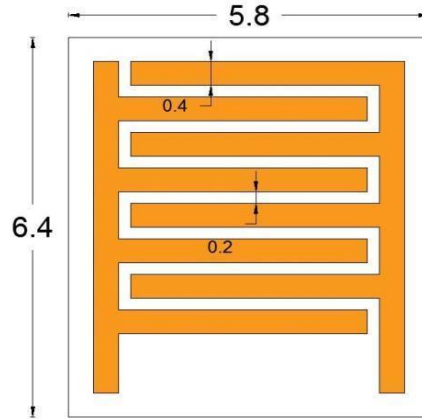


Figure 5. Geometry of EA pad used in validation case (all dimensions are in mm)

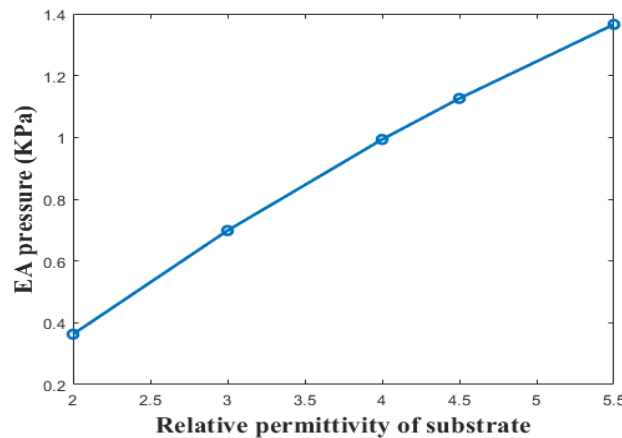


Figure 6. Modelled EA force versus relative permittivity of substrate for validation case

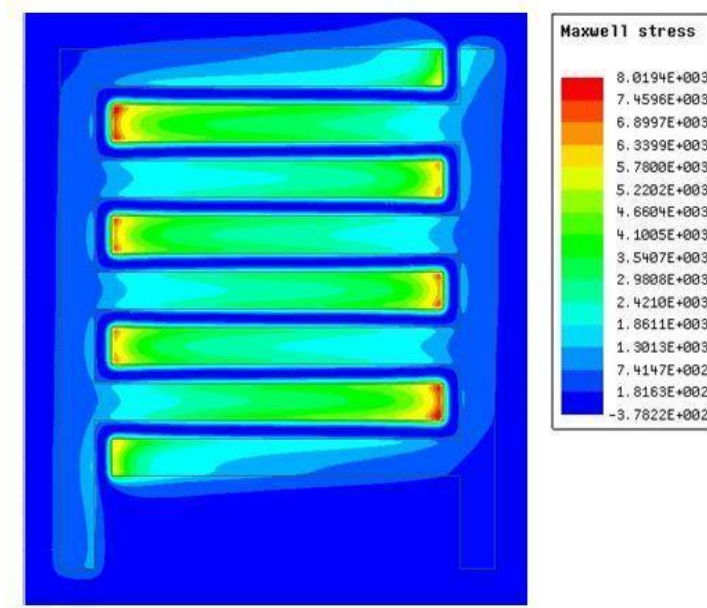


Figure7. Maxwell stress distribution of EA pad with substrate permittivity of 5.5

3. Results

3.1. 2D simulations

The 2D interdigitated EA pad simulations were carried out using ANSYS Maxwell software. The parametric geometry of interest was designed (see Figure 8) and in order to investigate the effects of electrode widths and spacings on the Maxwell stress tensor distribution and obtainable EA force, other parameters were kept constant and only the electrode widths and space between electrodes allowed to vary. Table 3 shows details of the parameters used for the 2D simulations. Figure 9 shows the Maxwell stress distribution on the line slightly above the interface of the air and substrate layers. According to the Maxwell stress equation Eq. (2), the maximum Maxwell stress is expected to occur where the cross-product of electric field and electric field gradient reaches its maximum. Results show (see Figure 9) that by increasing the width of electrodes the intensity of the Maxwell distribution decreases but the peaks become wider and also as we kept the effective area constant the number of peaks decreased. Therefore there is an optimum electrode width needed to maximise the total attractive force generated for a specified effective area of an EA pad (see Figure 10). As can be seen from Figure 9 the smaller the spacing between electrodes, the higher the EA forces generated, although in reality this will be limited by practical considerations such as the fabrication process, and for each particular spacing between electrodes, there is an optimum electrode width. Also on a practical basis, electrode spacing will have a minimum safe value in order to avoid arcing during use and the minimum safe spacing will thus depend on the applied voltage, amongst other factors. Therefore the dielectric breakdown voltages of constituent materials also need to be considered when designing and building an EA pad. Dadkhah *et al.* [8] suggested a bi-layer electrode design in order to avoid dielectric breakdown for smaller electrode spacings. It must thus be noted that these values depend on the effective area, the dielectric thickness, the thickness of the air gap and the relative permittivity of the substrate which we considered constant here. Dadkhah *et al* [8] showed that the higher the thickness of the air gap, the wider electrode width is needed to optimise EA pads design. Also it is worth noting that we can consider an EA pad as a co-planar capacitor with complex geometry and thus to maximise the total capacitance of an EA pad, minimising the space between electrodes is required, within constraints of dielectric breakdown limitations and thus safe operation. Following [23, 27] the total capacitance of a co-planar capacitor can be calculated using a conformal mapping (CM) technique. To prove this, the potential distribution of a 2D EA system with 16 electrodes was simulated (Figure 11). As can be seen, in the middle of the system there are vertical equipotential lines with a value of zero between electrodes. Therefore, ignoring marginal effects, the total capacitance of the system can be approximated with acceptable accuracy

using a conformal mapping technique. The capacitance of a periodical section (see Figure 12) of a dielectric layer and a substrate of an EA system are then given by:

$$C_p = \varepsilon_0 \varepsilon_r L \frac{K(k_r)}{K(k'_r)} \quad (11)$$

where ε_r is relative permittivity of the dielectric layer or the substrate; L is length of electrodes; K is elliptic integral of the first kind; and k_r is given by:

$$k_r = \frac{\sinh\left(\frac{\pi w}{2h_r}\right)}{\sinh\left(\frac{\pi(\frac{w}{2}+s)}{2h_r}\right)} \sqrt{\frac{\sinh^2\left(\frac{\pi(\frac{3w}{2}+s)}{2h_r}\right) - \sinh^2\left(\frac{\pi(\frac{w}{2}+s)}{2h_r}\right)}{\sinh^2\left(\frac{\pi(\frac{3w}{2}+s)}{2h_r}\right) - \sinh^2\left(\frac{\pi w}{2h_r}\right)}} \quad (12)$$

where w is width of electrodes; s is space between electrodes; h is thickness of dielectric layer or substrate; and k'_r is given by:

$$k'_r = \sqrt{1 - k_r^2} \quad (13)$$

Finally, total capacitance of the system is given by:

$$C_{total} = (N - 1)C_{p(Dielectric\ layer)} + (N - 1)C_{p(substrate)} \quad (14)$$

As shown in Figure 13, the smaller the spacing between electrodes and the smaller the width of the electrodes, the higher the total capacitance of the system. These results are in agreement with findings reported by Huang et al. [28].

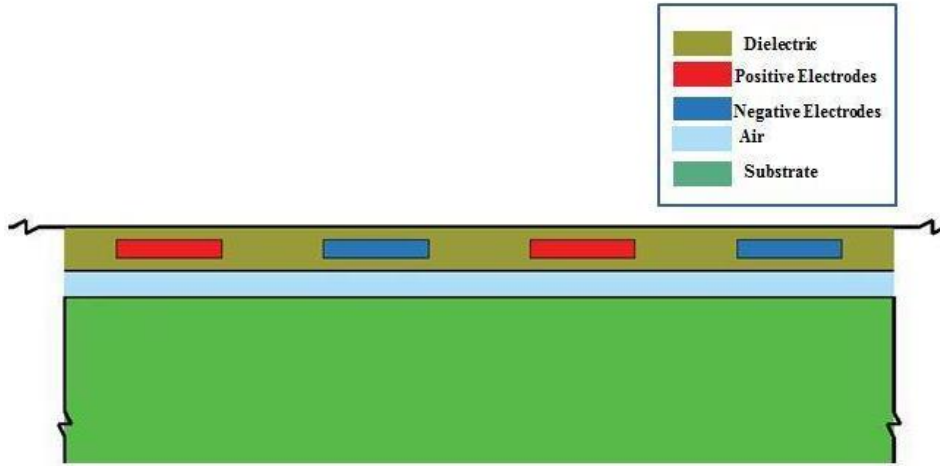


Figure 8. Schematic of 2D geometry of an interdigitated EA device

Table 3. Parameters for 2D interdigitated electroadhesive pad simulation

Voltage	Dual polarity	± 1 kV
Electrodes	Copper (perfect conductor)	Electrical Resistivity (ρ ohm \times m) = 0

Electrodes width	Varied	0.2 mm to 2 mm
Electrodes thickness	0.5 mm	
Space between electrodes	Varied	1 mm to 4 mm
Dielectric	$\epsilon_r=1000$	
Dielectric thickness	1 mm	
Layer between dielectric and substrate	Air	$\epsilon_r=1$
Thickness of air layer	0.5 mm	
Substrate	Glass	$\epsilon_r=4.6$
Substrate thickness	30 mm	
Effective pad surface area	36.2 mm \times 1 (dimensionless constant)	

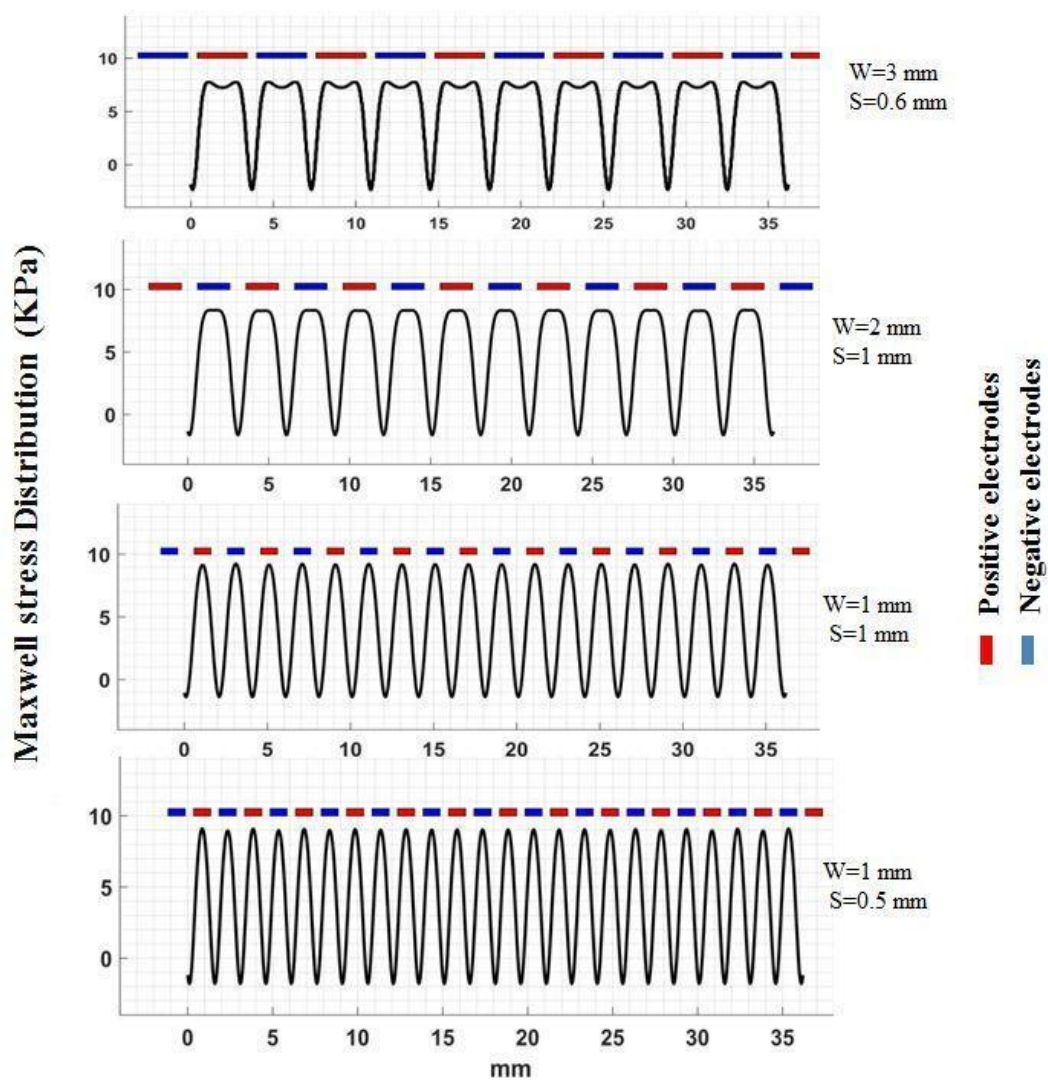


Figure 9. 2D Numerical investigation of the relationship between electrode parameters (width and spacing) and Maxwell stress distribution on nonconductive substrates.

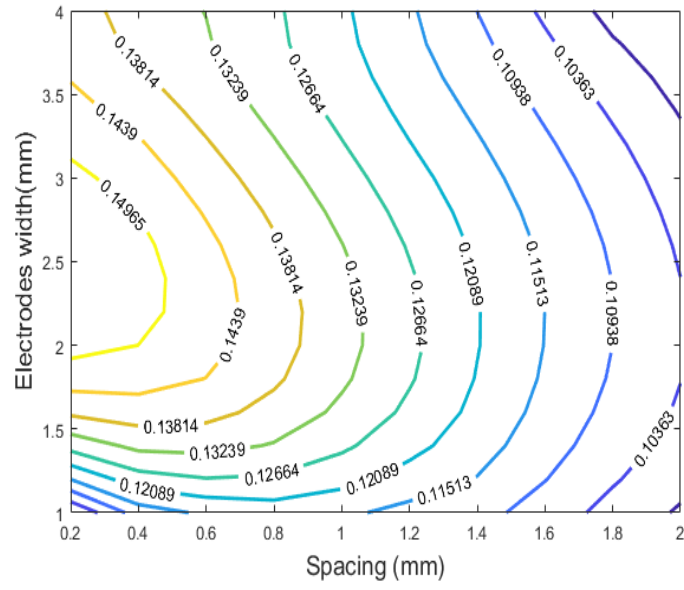


Figure 10. 2D Numerical investigation of the relationship between optimum electrode width and spacing to maximize obtainable EA force on non-conductive substrates

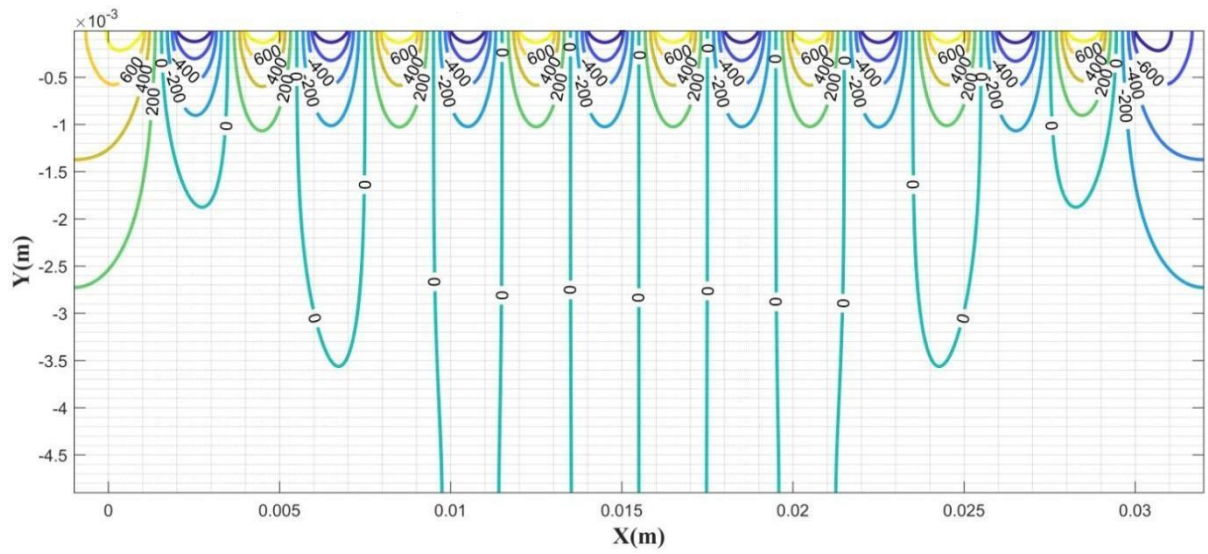


Figure 11. 2D Modelled potential distribution of coplanar capacitance with 16 electrodes

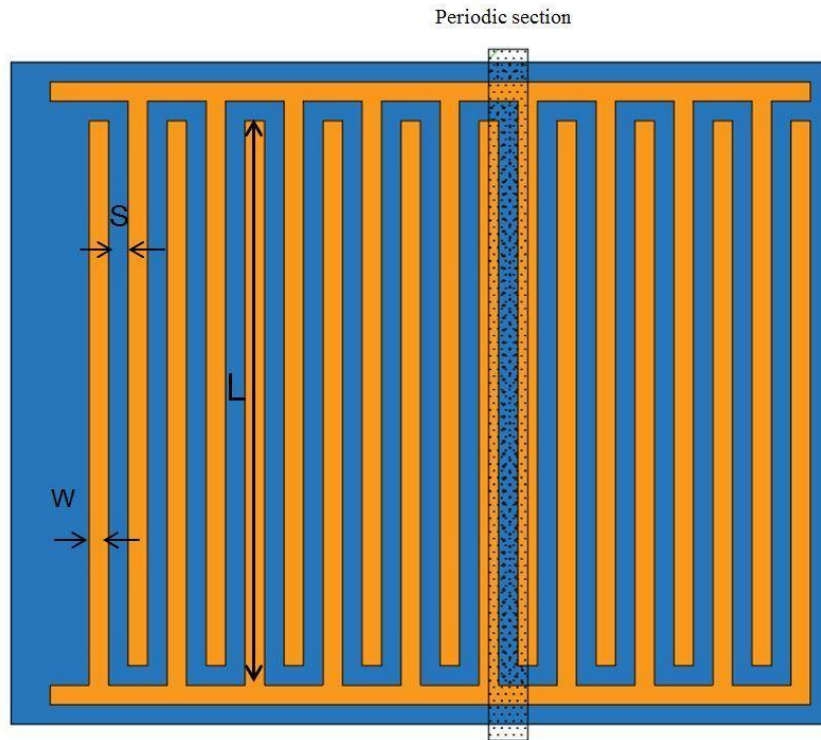


Figure 12. Schematic of coplanar capacitance showing simulated area and parameters

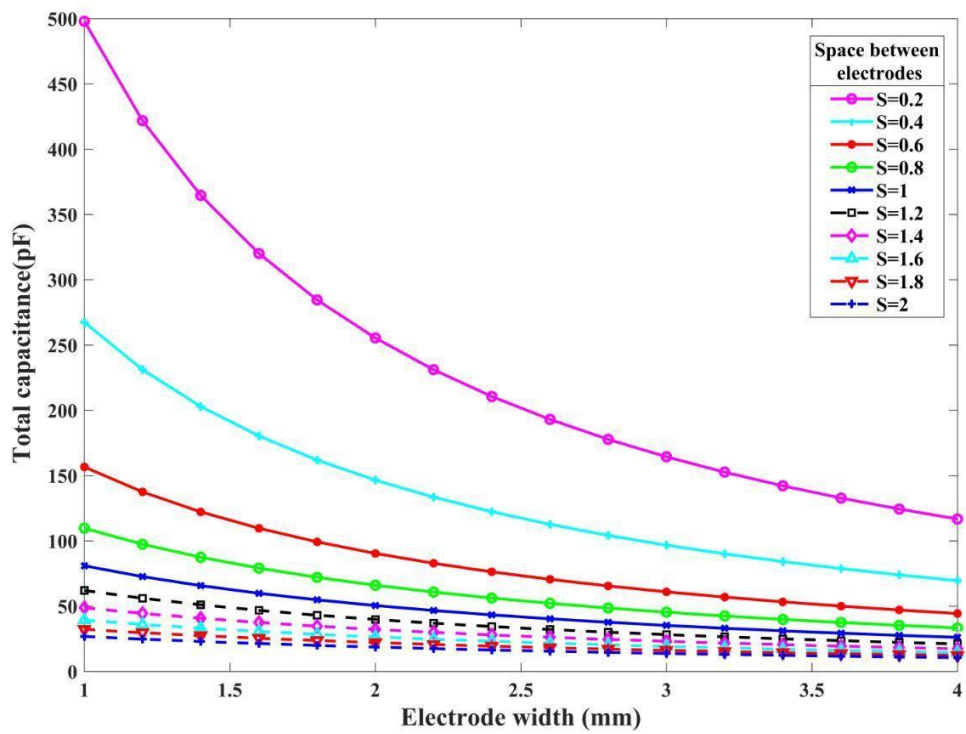


Figure 13. Relationship between capacitance of coplanar capacitor and electrode width and spacing

3.2. 3D simulations

Shape optimisation of EA pads has been carried out by designing seven different shapes while other parameters including effective area, electrode width, spacing between electrodes, and relative permittivities of both the dielectric layer and the substrate were kept constant (see table 4). First, two representative EA pads, (i) interdigitated and (ii) concentric circles were simulated to understand the relationship between electrode geometries and the generated EA forces. Simulation of the interdigitated electrode showed that the maximum EA pressure occurs at the corners of electrodes, which is due to maximisation of electric field and also electric field gradient in those areas. Therefore, at the next step, it was attempted to increase the EA force by increasing the number of electrode corners. The results show that although the number of maximum local pressures increases the total EA force for the whole interdigitated EA pad decreases. This means that electrode corners increase local pressures but have negative effects on the area nearby, and the net effect on the whole EA pad is deleterious. Simulation of electrodes in concentric circles reveals that the curved shape of the electrodes results in homogeneous pressure distribution and increased electric field gradient, resulting in higher EA force generation compared with simple interdigitated EA pads, which is in agreement with previous findings [12]. The next step was to decrease the sharpness of corners and use a half-hexagonal electrode shape. This was simulated and results show an improvement in the obtainable EA force. Finally, to combine both features, a sinusoidal electrode shape was designed and simulated. This provided the best performance between all designs studied here. Table 5 compares the obtainable attractive force and total capacity for different electrode structures; and Table 6 shows the effect of electrode shape on the electric field, electric field gradient and the Maxwell stress generated. It is noteworthy that 3D simulations of electroadhesion and particularly contour of electric field indicate those parts of EA pads in which dielectric breakdown occurs first. As an example in an interdigitated EA pad dielectric breakdown occurs in the right angles of electrodes. Capacitances of the new electrode designs are also calculated and results show that capacitance associated with sinusoidal and half-hexagonal shapes are higher than with other electrode geometries. A grid independency study for all of the simulations was carried out by applying 50% mesh refinement for each iteration to make sure that EA forces computed are independent of the number of elements. Table 7 shows statistical information of the last iteration of the 3D simulated interdigitated pad and figure 14 show convergence criteria (Energy error and delta energy) and also force computed and the number of elements for iterations.

Table 4. Parameters for 3D interdigitated electroadhesive pad simulation

Voltage	Dual polarity	± 1 kV
Electrodes width	1 mm	
Electrodes thickness	0.5 mm	
Space between electrodes	1 mm	
Dielectric	$\epsilon_r=1000$	
Dielectric thickness	1 mm	
Layer between dielectric and substrate	Air	$\epsilon_r=1$
Thickness of air layer	0.5 mm	
Substrate	Glass	$\epsilon_r=4.6$
Substrate thickness	30 mm	
Effective pad surface area	357 cm ²	

Table 5. The effect of electrodes design on obtainable attractive forces

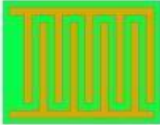
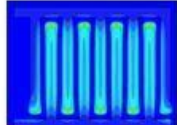
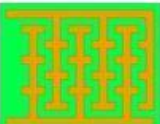
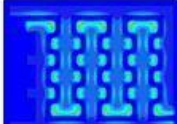
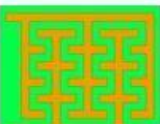
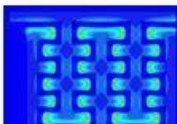
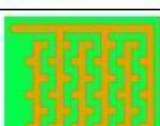
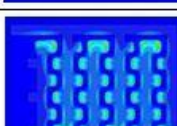






Pattern name	Shape of electrodes	Total area of electrodes(cm ²)	Total EA force (mN)	Total capacity (pF)	Maxwell stress
Interdigitated		146	14.483	962.69	
Interdigitated with teeth (1)		143	10.189	755.13	
Interdigitated with teeth (2)		146	11.381	835.57	
Interdigitated with teeth (3)		143	9.5595	712.43	
Concentric circles		142.17	15.031	1009	
Half-hexagonal		146	17.847	1279.7	
Sinusoidal shape		134	21.222	1700.8	

Table 6. The effect of electrode shapes on generated electric field and Maxwell stress distribution

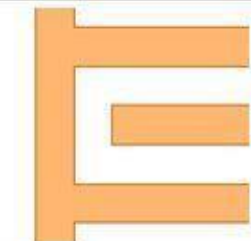
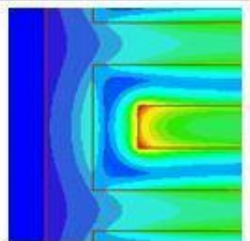
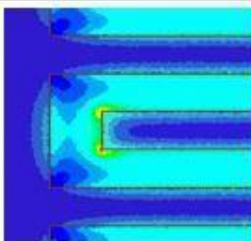
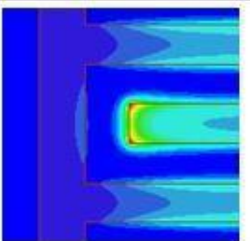
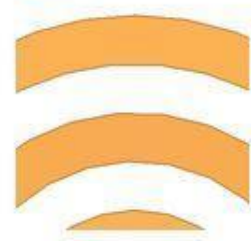
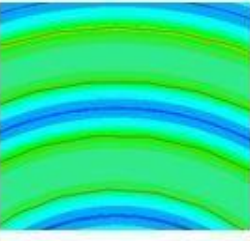
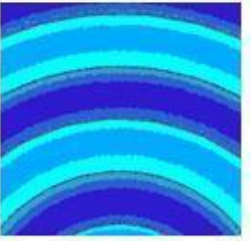
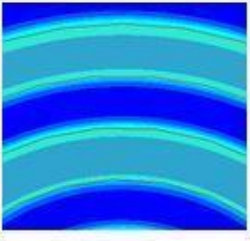
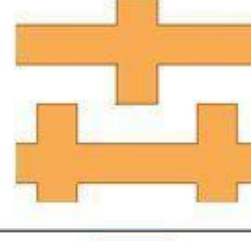
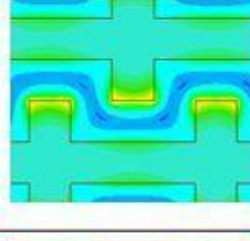
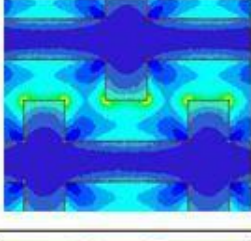
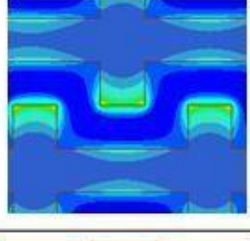
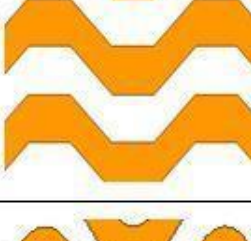
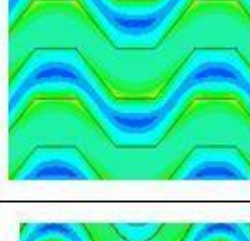
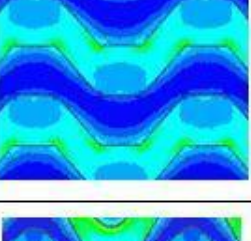
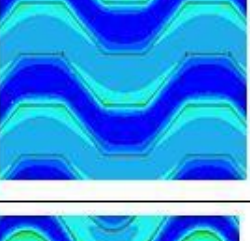
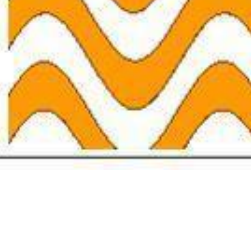
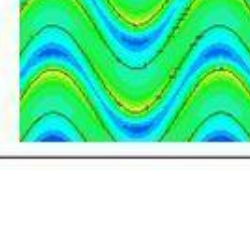
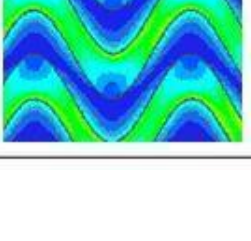
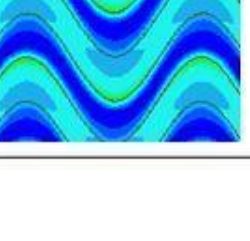
Electrodes shape	Magnitude of E- filed	Gradient of E-field in Z direction	Maxwell stress
			
			
			
			
			

Table 7. Statistical information of the grids generated for the last iteration of 3D modelled of the interdigitated pad

3D Mesh Statistics				
Geometry Name	Number of elements	Min edge length (mm)	Max edge length (mm)	Mean elements volume(mm ³)
Positive electrodes	1167164	0.00366118	0.174809	3.38E-06
Negative electrodes	1149252	0.00309745	0.161847	2.91E-06
Dielectric layer	14186716	0.00242048	0.148935	2.00E-06
Air	6409107	0.00682014	0.14254	2.79E-06
Substrate	3469347	0.0149766	0.677267	1.03E-04
Total number	26381586			

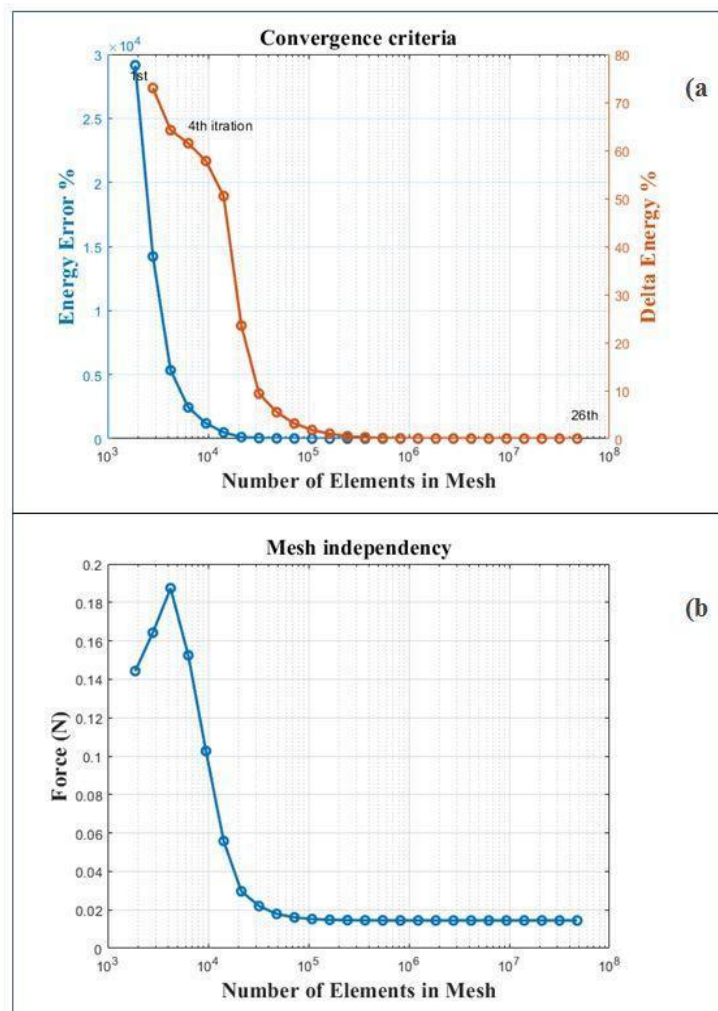


Figure14. a) Energy error and delta energy b) mesh independency of interdigitated EA pad simulation

4. Conclusions

We have carried out numerical simulations of electroadhesive (EA) electrode systems using FEA modelling to optimise electrode widths and spacings for a certain effective area, using the Maxwell stress criterion and based

on mathematical relationships between the generated EA forces and shapes of electrodes. New electrode shapes were designed and simulated. Simulations indicate that by decreasing the spacing between electrodes, higher EA forces are achievable and that for any particular spacing there is an optimum electrode width. New designed electrode shapes are promising for enhancing the obtainable EA forces and thus improving EA pad performance, with sinusoidal and half-hexagonal electrode designs giving considerable improvements compared with more established straight-interdigitated or concentric-circle electrode designs. The Maxwell stress contours presented in this work reveal the local Maxwell stress generated by different shapes of electrodes and can be used to support the design and optimisation of new EA device for future applications. Conformal mapping was used to find the relationship between electrode width and spacing in order to maximise total capacitance of the EA pad system.

Acknowledgements

This study was supported by Sheffield Hallam University through the Vice-Chancellor's PhD scholarship programme. The authors thank Jacques Penders for useful discussions.

References

- [1] Koh, K.H., Sreekumar, M. and Ponnambalam, S.G., *Mechatronics*, 35, 122 (2016).
<https://www.sciencedirect.com/science/article/pii/S0957415816000210>
- [2] Schmidt, D. and Berns, K., *Robotics and Autonomous Systems*, 61(12), 1288 (2013).
<https://doi.org/10.1016/j.robot.2013.09.002>
- [3] Monkman, G., *Industrial Robot: An International Journal*, 30(4), 326 (2003).
<https://www.emerald.com/insight/content/doi/10.1108/01439910310479595/full/html>
- [4] Shintake, J., Rosset, S., Schubert, B., Floreano, D. and Shea, H., *Advanced Materials*, 28(2), 231 (2016).
<https://onlinelibrary.wiley.com/doi/full/10.1002/adma.201504264>
- [5] Gao, X., Cao, C., Guo, J. and Conn, A., *Advanced Materials Technologies*, 4(1), 1800378(2019).
<https://onlinelibrary.wiley.com/doi/full/10.1002/admt.201800378>
- [6] Bamber, T., Guo, J., Singh, J., Bigharaz, M., Petzing, J., Bingham, P.A., Justham, L., Penders, J. and Jackson, M., *Journal of Physics D: Applied Physics*, 50(20), 205304 (2017).
<https://iopscience.iop.org/article/10.1088/1361-6463/aa6be4/meta>
- [7] Guo, J., Xiang, C. and Rossiter, J., *Materials & Design*, 156, 586(2018).
<https://www.sciencedirect.com/science/article/pii/S0264127518305574>
- [8] Dadkhah, M., Ruffatto III, D., Zhao, Z. and Spenko, M., *Journal of Electrostatics*, 91, 48 (2018).
<https://www.sciencedirect.com/science/article/pii/S0304388617301328>
- [9] Guo, J., Bamber, T., Chamberlain, M., Justham, L. and Jackson, M., *Journal of Physics D: Applied Physics*, 49(41), 4153049 (2016).
<https://iopscience.iop.org/article/10.1088/0022-3727/49/41/415304/meta>
- [10] Germann, J., Schubert, B. and Floreano, D., *IEEE/RSJ International Conference on Intelligent Robots and Systems*, 3933 (2014).
<https://ieeexplore.ieee.org/abstract/document/6943115>
- [11] Fessler, J., Mach, F. and Navrátil, J., *Open Physics*, 16(1), 430 (2018).
<https://www.degruyter.com/view/j/phys.2018.16.issue-1/phys-2018-0059/phys-2018-0059.xml?intcmp=trendmd&lang=de>

- [12] Ruffatto III, D., Shah, J. and Spenko, M., *Journal of Electrostatics*, 72(2), 147 (2014).
<https://www.sciencedirect.com/science/article/pii/S0304388614000084>
- [13] Guo, J., Taylor, M., Bamber, T., Chamberlain, M., Justham, L. and Jackson, M., *Journal of Physics D: Applied Physics*, 49(3), 035303 (2015).
<https://iopscience.iop.org/article/10.1088/0022-3727/49/3/035303>
- [14] Mao, J., Qin, L. and Zhang, W., *The Journal of Adhesion*, 92(4), 319 (2016).
<https://www.tandfonline.com/doi/full/10.1080/00218464.2015.1030014>
- [15] Melcher, J.R., Continuum electromechanics, Electromagnetic forces, force densities and stress tensor, (Cambridge. MIT Press, 198, pp.3.1 (1981).
- [16] Mao, J., Qin, L., Wang, Y., Liu, J. and Xue, L., *IEEE International Conference on Mechatronics and Automation*, 987 (2014).
<https://ieeexplore.ieee.org/abstract/document/6885832>
- [17] Liu, R., Chen, R., Shen, H. and Zhang, R., *International Journal of Advanced Robotic Systems*, 10(1), 36 (2013). <https://journals.sagepub.com/doi/full/10.5772/54634>
- [18] Cao, C., Sun, X., Fang, Y., Qin, Q.H., Yu, A. and Feng, X.Q., *Materials & Design*, 89, 485 (2016.).
<https://www.sciencedirect.com/science/article/pii/S0264127515305712>
- [19] Łapka, W., *Archives of Acoustics*, 43(1), 83 (2018).
<https://acoustics.ippt.pan.pl/index.php/aa/article/view/2111>
- [20] Chen, H. and Christensen, E.D., *Ocean Engineering*, 142, 597 (2017).
<https://www.sciencedirect.com/science/article/pii/S0029801817304043>
- [21] Woo, S.J. and Higuchi, T., *Journal of Applied Physics*, 108(10), 104906 (2010).
<https://aip.scitation.org/doi/full/10.1063/1.3487938>
- [22] Guo, J., Bamber, T., Hovell, T., Chamberlain, M., Justham, L. and Jackson, M., *IFAC-PapersOnLine*, 49(21), 309 (2016).
<https://www.sciencedirect.com/science/article/pii/S2405896316321644>
- [23] Nassr, A.A., Ahmed, W.H. and El-Dakhkhni, W.W., *Measurement science and technology*, 19(7), 075702 (2008).
<https://iopscience.iop.org/article/10.1088/0F957-0233/19/7/075702>
- [24] Yu, Y., Han, D., Wang, Y., Wang, F., Chen, X., Lyu, P., Guo, B., Shen, C., Zhang, Q. and Li, Y., *Journal of Instrumentation*, 14(07), P07020 (2019).
<https://iopscience.iop.org/article/10.1088/1748-0221/14/07/P07020/meta>
- [25] Tajdari, T., Fua'ad bin Rahmat, M. and Thuku, I.T., *IEEE International Conference on Control System, Computing and Engineering*, 194(2012)
<https://ieeexplore.ieee.org/abstract/document/6487140>
- [26] Engineering ToolBox, (2010). Relative Permittivity - the Dielectric Constant. [online] Available at: https://www.engineeringtoolbox.com/relative-permittivity-d_1660.html [Accessed 02. 10. 2020].
- [27] Mak, K.W. and Hao, J., *International Journal of Advances in Applied Physics Research*, 1, 1 (2014).
<https://pdfs.semanticscholar.org/ec3e/2a1d77dff9218bf20d5d3c0ac0ff5a6cb9e9.pdf>

- [28] Huang, Y., Zhan, Z. and Bowler, N., *AIP Conference Proceedings*, 1806(1), 110017 (2017).
<https://aip.scitation.org/doi/abs/10.1063/1.4974695>